# Normal-state magnetic susceptibility in $TlSr_2(Lu_{1-x}Ca_x)Cu_2O_y$ from the underdoped to the overdoped regime

Takashi Kondo, Yoshimi Kubo, Yuichi Shimakawa, and Takashi Manako
*Fundamental Research Laboratories, NEC Corporation, 34, Miyukigaoka, Tsukuba 305, Japan*
(Received 18 November 1993)

Analyzing the normal-state magnetic susceptibility $\chi$ for $TlSr_2(Lu_{1-x}Ca_x)Cu_2O_y$, whose carrier density covers the entire range from the underdoped to the overdoped regime, as a function of Ca concentration $x$ and oxygen content $y$, we find significant correlations between $\chi$ and the carrier density. (1) The temperature dependence of $\chi$ gradually changes from positive to negative on going from the underdoped to the overdoped regime. It is almost entirely temperature independent at the optimum carrier density (maximum $T_c$). (2) The magnitude of $\chi$ gradually increases with the carrier density. For the optimum carrier density, the spin susceptibility at 200 K is estimated to be about $1.2\times10^{-4}$ emu/mol Cu. These characteristics are typical of most high-$T_c$ cuprates and seem to be closely related to the high-$T_c$ superconductivity mechanism.

## I. INTRODUCTION

The normal-state physical properties of high-$T_c$ cuprates have been extensively investigated in efforts to elucidate the high-$T_c$ superconductivity mechanism. The underdoped regime, where $T_c$ increases with carrier density, has been explored in many studies using various kinds of high-$T_c$ cuprates. Research into the overdoped regime, however, where $T_c$ decreases with carrier density, is as yet insufficient because of the smaller number of overdoped high-$T_c$ cuprates. Although the well-known $La_{2-x}Sr_xCuO_4$ system can be overdoped for $x>0.15$,[1] there remains controversy as to whether the overdoped materials are homogeneous or not.[2,3] Recently, we have revealed that $Tl_2Ba_2CuO_{6+\delta}$ (Refs. 4 and 5) and $TlSr_2CaCu_2O_{7-\delta}$ (Refs. 6 and 7) can be overdoped by oxygen nonstoichiometry from high-$T_c$ superconductors to metallic nonsuperconductors. Since these materials show neither phase transition nor inhomogeneity, they are suitable for studying the overdoped regime. While their normal-state transport properties have been studied in detail,[8-10] their normal-state magnetic properties have not. The large Curie term of the magnetic susceptibility for $Tl_2Ba_2CuO_{6+\delta}$,[8] which is probably caused by the $Cu^{2+}$ ion replacing the Tl site, prevents us from determining the intrinsic spin susceptibility of the $CuO_2$ plane in the overdoped regime. In this respect, $TlSr_2CaCu_2O_{7-\delta}$ is more favorable because of its much smaller Curie term.[7] In addition, the carrier density of $TlSr_2CaCu_2O_{7-\delta}$ can be reduced by replacing Ca with Y or rare-earth elements, covering the entire underdoped regime. Therefore, the carrier density of $TlSr_2(R_{1-x}Ca_x)Cu_2O_y$ ($R$=Y or rare-earth metals) can be changed to cover the wide range from the underdoped to the overdoped regime, by changing the cation substitution and oxygen nonstoichiometry.[11]

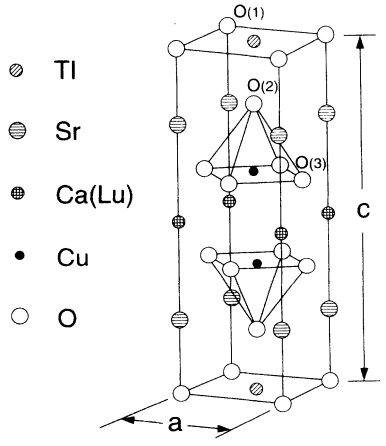


FIG. 1. Model crystal structure for $TlSr_2(Lu_{1-x}Ca_x)Cu_2O_y$ (tetragonal, space group $P4/mmm$).

$TlSr_2(R_{1-x}Ca_x)Cu_2O_y$, in contrast to $La_{2-x}Sr_xCuO_4$, has two $CuO_5$ square-pyramidal layers per formula unit, similar to those in $YBa_2Cu_3O_{7-\delta}$ and $Bi_2Sr_2CaCu_2O_8$. An important point is that $TlSr_2(R_{1-x}Ca_x)Cu_2O_y$ is the only pyramidal system that changes from an insulator to an overdoped metal when it is doped. It also does not contain a CuO chain layer like that in $YBa_2Cu_3O_{7-y}$. Moreover, the relatively simple crystal structure (tetragonal $P4/mmm$) of $TlSr_2(R_{1-x}Ca_x)Cu_2O_y$ (Fig. 1), which is independent of the doping level, should be an advantage in studying physical properties.

This paper describes the preparation, superconductivity, and normal-state magnetic susceptibility of $TlSr_2(Lu_{1-x}Ca_x)Cu_2O_y$, from the underdoped to the overdoped regime. Lutetium was selected because $Lu^{3+}$ is nonmagnetic, and because it was easier to prepare single-phase samples when using it than when using another nonmagnetic ion, $Y^{3+}$.

## II. SAMPLE PREPARATION AND CHARACTERIZATION

$TlSr_2(Lu_{1-x}Ca_x)Cu_2O_y$ samples with $x=0$, 0.1, 0.2, 0.3, 0.4, 0.5, 0.6, 0.7, and 1.0 were prepared by the solid-

 

state reaction of 99.999% pure CaO (Johnson & Matthey), 99.999% pure CuO (Johnson & Matthey), 99.995% pure $Tl_2O_3$ (Johnson & Matthey), 99.9% pure $Lu_2O_3$ (Shin-etsu Chemical), and 99% pure SrO (High Purity Chemetals) powders. Before the as-received SrO and CaO powders were used, their formula weights were calibrated by thermogravimetric, titrimetric, and spectroscopic analyses. It is not easy to prepare single-phase $TlSr_2(Lu_{1-x}Ca_x)Cu_2O_y$ because the volatility of thallium makes it difficult to keep stoichiometry at the sintering temperature. Therefore, we started with Tl-rich compositions and adjusted the final Tl compositions by measuring the sample weight. Except for the samples with $x=1.0$, the SrO, CaO, $Lu_2O_3$, and CuO powders were thoroughly mixed with stoichiometric compositions using an agate mortar. For $x=1.0$, a Ca-poor composition (Sr:Ca:Cu=2:0.85:2) was used because the Ca site was found to be partially substituted with Tl.[6,7,12] The mixed powders were dried at about 350 °C for 5 h in flowing oxygen and then mixed with the $Tl_2O_3$ powder in Tl-rich compositions. The excess amounts of Tl were 20% for $x=0.1$ and 0.2, 40% for $x=0.3$ and 0.4, and 70% for $x\geq 0.5$. Then the mixtures were pressed into pellets and each pellet was wrapped with gold foil. This process was performed in a dry box with a nitrogen atmosphere. The pellets were sintered at 890–940 °C for 1–5 h and the Tl loss during sintering was estimated by weighing. The sintering was repeated 2–3 times, with intermediate grinding, pressing, and wrapping, until weighing indicated that the Tl composition was stoichiometric. For $x=1.0$, the final Tl composition was adjusted to about 1.2, since Tl partly occupies the Ca site in addition to the Tl site. In fact, for $x=1.0$, a single-phase sample was obtained only for such a nonstoichiometric composition. Each of these synthesized samples was confirmed to be a single-phase sample by powder x-ray diffraction. Fully oxygenated samples were obtained by annealing at 350 °C for 10 h in flowing oxygen.

Scanning electron microscopy (SEM) and electron-probe microanalysis (EPMA) were performed using a JEOL superprobe JXA-8600MX to survey the sample homogeneity and to determine the chemical composition for each sample. The standards used for EPMA (wavelength-dispersive x-ray analysis) were $Tl_2O_3$, $SrTiO_3$, $CaF_2$, $LuP_5O_{14}$, and Cu metal. The average composition for each starting composition $x$ is listed in Table I, in which each composition is normalized so as to yield six cations per formula unit. Sample homogeneity was confirmed by analyzing about ten different points for each sample. Moreover, backscattered-electron (compositional) imaging for each sample indicated no impurity phase within the crystalline grains or on the grain boundaries. The composition of the $x=1.0$ sample was Tl-rich and Ca-poor, suggesting that the Ca site was substituted with Tl.

Powder x-ray-diffraction data were collected by using a Rigaku Geigerflex diffractometer and a Cu $K\alpha$ radiation source (12.5 kW) with a curved graphite monochromator. The diffractometer was stepped by 0.02° in $2\theta$ at every 4 s over $5°<2\theta<90°$ with a slit width of 0.5°. The results were refined using the Rietveld analysis program RIETAN.[13] The observed and calculated diffraction patterns for representative samples ($x=0$, 0.4, 0.7, and 1.0) are shown in Figs. 2(a)–2(d). The peaks of each observed pattern could be all assigned to the peaks for the crystal-structure model, tetragonal space group $P4/mmm$. No impurity peaks were observed. As shown in Figs. 2(a)–2(d), in each pattern the ratio of the height of the (102) reflection peak to that of the (101) reflection peak increases as the amount of Ca substituted for Lu increases. The peak heights for (003), (111), and (112) reflection also change significantly with the amount of substitution. In the Rietveld analysis, the thermal parameters ($B$) were assumed to be isotropic. Because the samples include heavy atoms such as Tl and Lu, it is difficult to refine the occupation factors ($g$) for the oxygen ions. Thus, only the occupation factors of the metal ions were considered and the occupation factors of the oxygen ions were fixed at 1.0. The resulting large isotropic thermal parameter ($\approx 2.0$) for Tl, which was first located at an ideal $1b$ site, suggested that the Tl atom had been displaced. Therefore, the Tl site was split into four pieces by assigning a $4m$ site deviating slightly from the ideal site.[6] The occupation factor of the copper ion was also fixed at 1.0 because it could not be refined together with the isotropic thermal parameter for Cu. The final refined structural parameters and $R$ factors for the oxygenated samples are listed in Table II. For the $x=1.0$ sample, the Ca site was refined assuming that it was partially substituted with Tl. This result was consistent with the EPMA data presented in Table I. The $g$ values of the Ca sites for the $x=0.6$ and $x=0.7$ samples were found to be fairly small compared with the designed compositions. This suggests that the Ca sites of these samples are partly substututed with Tl as well as Lu, as occurred in the $x=1.0$ sample. This partial substitution is corroborated

TABLE I. Chemical compositions from SEM-EPMA data for the $TlSr_2(Lu_{1-x}Ca_x)Cu_2O_y$ samples. The results are normalized to yield six cations per formula unit. Numbers in parentheses are estimated standard deviations of the last significant digit.

| | $x=0$ | $x=0.1$ | $x=0.2$ | $x=0.3$ | $x=0.4$ | $x=0.5$ | $x=0.6$ | $x=0.7$ | $x=1.0$ |
|---|---|---|---|---|---|---|---|---|---|
| Tl | 0.97(5) | 0.97(2) | 1.04(3) | 0.98(2) | 0.99(1) | 1.01(2) | 1.05(2) | 1.07(2) | 1.25(2) |
| Sr | 2.04(5) | 1.99(5) | 1.98(3) | 2.05(3) | 2.03(1) | 2.00(2) | 2.02(3) | 2.04(2) | 1.99(3) |
| Ca | | 0.12(1) | 0.22(3) | 0.26(1) | 0.36(1) | 0.47(1) | 0.53(1) | 0.61(1) | 0.77(3) |
| Lu | 0.94(2) | 0.90(2) | 0.78(2) | 0.68(2) | 0.57(1) | 0.49(3) | 0.42(3) | 0.29(1) | |
| Cu | 2.05(4) | 2.02(4) | 1.98(3) | 2.03(2) | 2.05(2) | 2.03(2) | 1.98(4) | 1.99(3) | 1.99(2) |

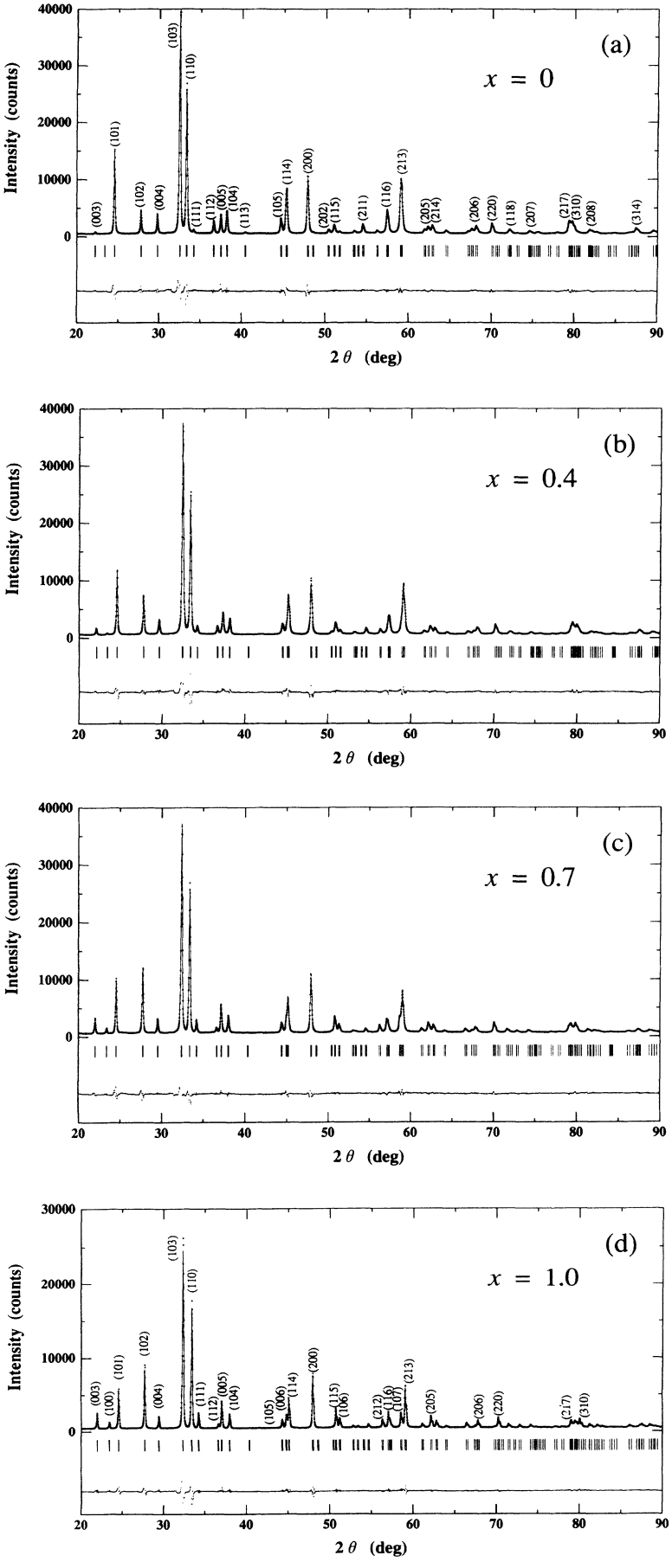


FIG. 2. Rietveld refinement patterns for $TlSr_2(Lu_{1-x}Ca_x)Cu_2O_y$: (a) oxygenated sample with $x=0$ and $T_c<2$ K (insulator), (b) oxygenated sample with $x=0.4$ and $T_c=64$ K, (c) argon-reduced sample with $x=0.7$ and $T_c=78$ K, and (d) oxygenated sample with $x=1.0$ and $T_c<2$ K (metal). Dots are observed intensities and solid lines are calculated intensities. Vertical marks below the profile indicate the positions of the allowed reflections. The curve at the bottom shows the difference between the observed and calculated intensities on the same scale.

TABLE II. Refined structural parameters from powder x-ray-diffraction data at room temperature for the oxygenated $TlSr_2(Lu_{1-x}Ca_x)Cu_2O_y$ samples. The crystal structures of all samples have $P4/mmm$ space-group symmetry. The atom positions are Tl $4m[x,0,0.5]$, Sr $2h[0.5,0.5,z]$, Ca $1c[0.5,0.5,0]$, Lu $1c[0.5,0.5,0]$, Cu $2g[0,0,z]$, O(1) $1d[0.5,0.5,0.5]$, O(2) $2g[0,0,z]$, O(3) $4i[0,0.5,z]$. The occupation factors of copper and oxygen ions are set at 1.0. Numbers in parentheses are estimated standard deviations of the last significant digit. The relative changes in oxygen content per formula unit are given in the last row (see text).

| Parameter | | $x=0$ | $x=0.1$ | $x=0.2$ | $x=0.3$ | $x=0.4$ | $x=0.5$ | $x=0.6$ | $x=0.7$ | $x=1.0$ |
|---|---|---|---|---|---|---|---|---|---|---|
| $a=b$ (Å) | | 3.795 92(6) | 3.793 27(7) | 3.791 68(6) | 3.789 77(8) | 3.788 06(7) | 3.787 65(8) | 3.784 75(8) | 3.784 41(7) | 3.783 40(6) |
| $c$ (Å) | | 11.975 0(2) | 11.994 3(2) | 12.007 7(2) | 12.020 2(3) | 12.029 1(2) | 12.044 6(3) | 12.058 6(3) | 12.075 8(2) | 12.116 4(2) |
| Tl | $g$ | 0.25 | 0.25 | 0.25 | 0.25 | 0.25 | 0.25 | 0.25 | 0.25 | 0.25 |
| | $x$ | 0.071(4) | 0.07 | 0.07 | 0.075(4) | 0.07 | 0.076(4) | 0.08 | 0.083(3) | 0.085(3) |
| | $B$ (Å$^2$) | 0.24(22) | 0.28(15) | 0.32(13) | 0.14(25) | 0.41(14) | 0.35(26) | 0.23(15) | 0.27(22) | 0.37(23) |
| Sr | $g$ | 1.0 | 1.02(2) | 1.0 | 1.0 | 1.0 | 1.0 | 1.0 | 0.98(2) | 0.98(2) |
| | $z$ | 0.290 1(4) | 0.290 0(4) | 0.290 4(4) | 0.290 0(5) | 0.289 8(5) | 0.288 7(5) | 0.289 0(4) | 0.288 8(4) | 0.288 2(4) |
| | $B$ (Å$^2$) | 0.32(13) | 0.66(19) | 0.59(14) | 0.49(16) | 0.37(16) | 0.50(17) | 0.63(16) | 0.44(14) | 0.49(22) |
| Ca[a] | $g$ | | 0.14(2) | 0.23(2) | 0.31(2) | 0.37(2) | 0.48(2) | 0.56(2) | 0.62(1) | 0.83(1) |
| | $B$ (Å$^2$) | | 0.54(18) | 0.53(19) | 0.46(22) | 0.44(23) | 0.46(28) | 0.42(28) | 0.42(28) | 0.37(36) |
| Lu[a,b] | $g$ | 1.0 | 0.86(2) | 0.77(2) | 0.69(2) | 0.63(2) | 0.52(2) | 0.44(2) | 0.38(1) | 0.17(1)[b] |
| | $B$ (Å$^2$) | 0.83(12) | 0.54(18) | 0.53(19) | 0.46(22) | 0.44(23) | 0.46(28) | 0.42(28) | 0.42(28) | 0.37(36)[b] |
| Cu | $z$ | 0.135 7(6) | 0.137 1(6) | 0.137 2(6) | 0.137 3(6) | 0.137 7(6) | 0.137 5(7) | 0.138 5(6) | 0.138 4(6) | 0.139 5(6) |
| | $B$ (Å$^2$) | 0.64(24) | 0.66(25) | 0.83(24) | 0.77(26) | 0.61(25) | 0.64(27) | 0.81(24) | 0.81(23) | 0.65(22) |
| O(1) | $B$ (Å$^2$) | 2.2(12) | 2.2(12) | 2.2(12) | 2.3(14) | 1.5(13) | 2.2(15) | 2.1(14) | 2.3(14) | 3.9(17) |
| O(2) | $z$ | 0.326(3) | 0.319(3) | 0.323(3) | 0.326(3) | 0.324(3) | 0.328(3) | 0.326(3) | 0.331(3) | 0.333(3) |
| | $B$ (Å$^2$) | 2.6(10) | 4.2(11) | 3.0(10) | 2.5(11) | 3.7(12) | 1.8(12) | 2.9(11) | 2.2(10) | 1.8(10) |
| O(3) | $z$ | 0.117(2) | 0.118(2) | 0.119(2) | 0.120(2) | 0.120(2) | 0.122(2) | 0.122(2) | 0.124(2) | 0.128(2) |
| | $B$ (Å$^2$) | 0.72(52) | 0.63(52) | 0.71(53) | 0.56(58) | 0.75(58) | 0.56(62) | 0.72(57) | 0.80(56) | 1.51(66) |
| $R_{wp}$ (%) | | 4.65 | 4.33 | 4.70 | 4.78 | 4.81 | 4.94 | 4.70 | 4.65 | 5.88 |
| $R_{ex}$ (%) | | 2.87 | 2.83 | 2.83 | 2.73 | 2.75 | 2.77 | 2.74 | 2.73 | 4.52 |
| $\Delta y$ | | | 0.040 | 0.035 | 0.078 | 0.060 | 0.071 | 0.088 | 0.070 | 0.102 |

[a]Constraints: $g(Ca)+g(Lu)=1$; $B(Ca)=B(Lu)$.

[b]Tl(2) $1c[0.5,0.5,0]$ for the $x=1.0$ sample (see text). Constraints: $g(Ca)+g[Tl(2)]=1$; $B(Ca)=B[Tl(2)]$.

by the fact that the EPMA data for these samples also indicate Tl-rich and Ca-poor compositions.

## III. OXYGEN NONSTOICHIOMETRY AND SUPERCONDUCTIVITY

In order to investigate the effect of oxygen content on the superconducting properties, the oxygenated samples were reduced in flowing argon at various temperatures up to 550 °C for 5 h. This reduction caused little change of the x-ray-diffraction pattern, and resulted in no new phases or structural changes.

The relative change in oxygen content was determined from the weight difference between the oxygenated and argon-reduced samples. The weight of each oxygenated sample decreased during annealing in flowing argon, and the reversibility of the weight change was checked by reannealing the sample at 350 °C in flowing oxygen. The sample weight was almost completely recovered when the argon-annealing temperature $T_a$ was less than 450 °C, but it was not entirely recovered when $T_a$ was greater than 450 °C. This unrecovered weight was attributed to the sublimation of Tl because it increased with $T_a$. The unrecovered weight was as small as 0.15 wt. % even for the maximum $T_a$ of 550 °C, from which the amount of Tl sublimation was estimated to be 0.005 per formula unit. Such small amount of Tl sublimation never changed the crystal structure parameters nor physical properties after oxygen reannealing. Thus, the relative change in oxygen content was determined by the weight increase during the oxygen reannealing.

The oxygen content is an important parameter for doping in the $TlSr_2(Lu_{1-x}Ca_x)Cu_2O_y$ system.[11] For $x=1.0$, for example, a change in $y$ as small as 0.1 per formula unit yielded a large $T_c$ change of about 70 K. The $T_c$ change was confirmed to be reversible for all samples even when the weight change was not reversible.

The lattice parameters $a$ and $c$ determined by the Rietveld refinements for both oxygenated and argon-reduced samples are plotted in Figs. 3(a) and 3(b) against the designed Ca concentration $x$. For the oxygenated samples, the $c$ axis linearly elongates by about 1.2% as $x$ increases, whereas the $a$ axis shrinks by only about 0.3%. The argon reduction stretches the $a$ axis but changes the $c$ axis length only a little. The linear increase in $c$ versus $x$ indicates that the $Lu^{3+}$ ion (ionic radius 0.97 Å) is systematically substituted by the larger $Ca^{2+}$ ion (1.12 Å). This systematical substitution is also supported by the fact that the $z$ component of the O(3) site systematically increases from $x=0$ to $x=1.0$ as shown in Table II. The difference in $c$ between the $x=0$ and $x=1.0$ samples, about 0.14 Å, is consistent with the difference in the ionic diameters between $Lu^{3+}$ and $Ca^{2+}$ (0.30 Å), considering the angle of elevation between $Lu^{3+}/Ca^{2+}$ and $O^{2-}(3)$ in the neighboring $CuO_2$ plane ($\approx 37°$). The lattice parameter $c$ thus appears to be determined mainly by the ionic radii of $Lu^{3+}$ and $Ca^{2+}$.

The lattice parameter $a$, on the other hand, seems to be determined mainly by covalent Cu-O bonding, which depends on the carrier density in the $CuO_2$ plane. In general, hole doping should decrease the Cu-O bond length because it reduces the number of electrons in the Cu-O antibonding band. This is clearly demonstrated in Fig. 3(a), in which the $a$ axis shrinks with hole doping through Ca substitution and stretches with "electron" doping through argon reduction. With argon reduction, the lattice parameter $c$ decreases when $x<0.6$, whereas it increases when $x=1.0$. This suggests that there is no correlation between the lattice parameter $c$ and the carrier density.

Magnetization data were obtained down to 5 K at a magnetic field of 1 Oe by using a Quantum Design superconducting quantum interference device magnetometer. All measurements were performed on bulk samples of about $4\times3\times1$ mm$^3$. Figure 4 shows the Meissner signals (field cooled) for the samples when $0.1\le x\le0.6$. The shielding signal (zero-field cooled) is presented only for the $x=0.1$ argon-reduced sample because the Meissner signal is very small. All oxygenated samples show narrow transition widths (10–90% of complete transition), 2–8 K, and no change in low-temperature signals. This verifies the sample homogeneity indicated by the SEM-EPMA data. The $x=0$ oxygenated sample shows no superconducting transition down to 2 K, and its resistivity exhibits semiconducting temperature dependence. Argon-reduced samples show transition-width broadenings and small tails near $T_c$, both of which may be caused by inhomogeneous oxygen distribution. Such slight inhomogeneity, however, will not significantly affect the bulk properties such as magnetic susceptibility. Thus we define the $T_c$ value as the temperature at which the Meissner signal becomes 10% of that at 5 K. Except for the $x=0.1$ argon-reduced sample, all samples show large Meissner fractions of 40–80%. These samples also show large shielding signals with apparent volume fractions above 100%, which can be explained in terms of the estimated demagnetizing factor, $n\approx0.2$, and the bulk shielding current. These facts clearly assure the bulk superconductivity of these samples. The small shielding fraction ($\approx25\%$) of the $x=0.1$ argon-reduced sample ($T_c\approx7$ K) suggests the coexistence of the insulating phase.

In Fig. 3(c), $T_c$ values for the $TlSr_2(Lu_{1-x}Ca_x)Cu_2O_y$ samples oxygenated at 350 °C and argon-reduced at 550 °C, which is the strongest reduction in this work, are plotted against the Ca concentration $x$. The relative change in oxygen content per formula unit between the oxygenated and argon-reduced samples for each concentration $x$ is given as $\Delta y$ in Table II. It should be noted that the oxygen nonstoichiometry causes significant changes in superconductivity. When $x$ increases from 0 to 1.0, the oxygenated sample changes, by way of a superconductor showing a maximum $T_c$ value of 72 K at

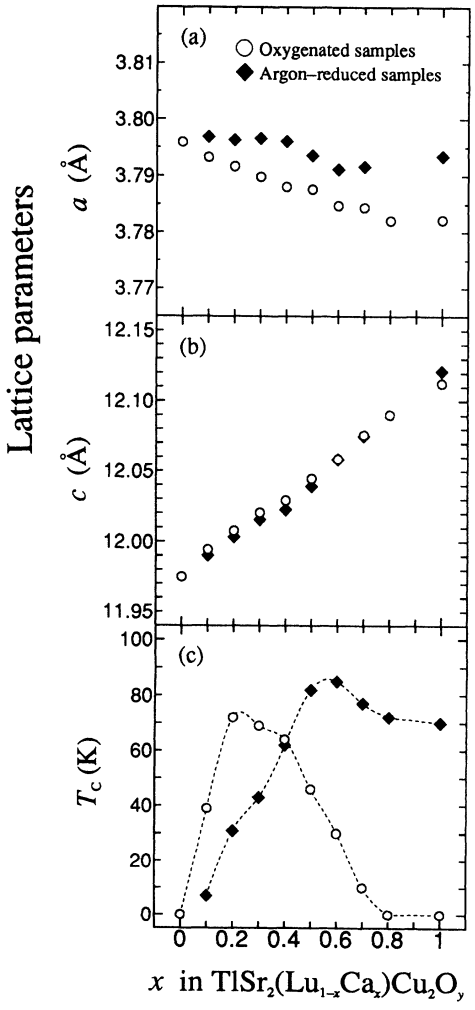


FIG. 3. Lattice parameters $a$ (a) and $c$ (b), and $T_c$ values (c) plotted against the Ca concentration $x$ for $TlSr_2(Lu_{1-x}Ca_x)Cu_2O_y$. Open circles and closed diamonds represent samples oxygenated at 350 °C and argon reduced at 550 °C, respectively. The data for $x=0.8$ are taken from Ref. 11.

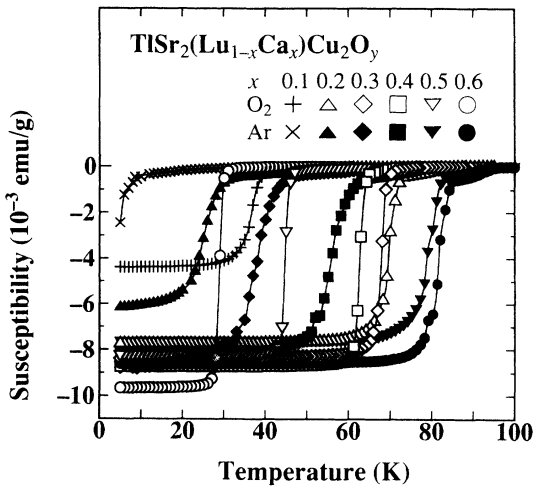


FIG. 4. Meissner signals at a magnetic field of 1 Oe for $TlSr_2(Lu_{1-x}Ca_x)Cu_2O_y$ with $0.1\le x\le0.6$. Open and closed symbols represent samples oxygenated at 350 °C and argon reduced at 550 °C, respectively. The shielding signal is shown for the $x=0.1$ argon-reduced sample (×) (see text).

$x=0.2$, from an insulator ($x=0$) to a nonsuperconducting metal ($x=1.0$). As the oxygen content $y$ decreases with argon reduction, the $T_c$ value monotonically decreases when $x \leq 0.2$, whereas it increases when $x \geq 0.6$. This means that the samples for which $x \leq 0.2$ and $x \geq 0.6$ belong to the underdoped and the overdoped regimes, respectively. For $0.3 \leq x \leq 0.5$, however, the $T_c$ value changes with argon reduction from the overdoped to the underdoped regime, taking a maximum value at an intermediate oxygen content. For example, the $x=0.4$ sample shows a $T_c$ of above 80 K with moderate argon reduction at 450 °C.

To estimate the carrier density precisely, it is necessary to have accurate values for both $x$ and $y$. Although each $y$ value has not been determined in the present work, some estimates can be taken from the earlier work.[6] For the previous sample with the designed composition $x=1.0$, the neutron-diffraction study revealed that $x=0.88$ and $y=6.88$ for the oxygenated sample (the nonsuperconducting metal) and that $x=0.88$ and $y=6.80$ for the argon-reduced sample ($T_c=58$ K in the overdoped regime). These values can be used to calculate a doped hole carrier density per $CuO_2$ plane of 0.32 for the oxygenated sample and 0.24 for the argon reduced sample. The Hall coefficient measurement[7] also showed that the hole carrier density was decreased by argon reduction. However, the "hole carrier densities" calculated from the Hall coefficient are, respectively, 2.2 and 1.2 per $CuO_2$ plane, which are five times or more bigger than those calculated from the chemical composition. Such discrepancy between chemical doping and the Hall coefficient strongly suggests that the "doped Mott insulator" picture is broken down, at least in the overdoped regime. In the usual metal, the Hall coefficient is determined by the Fermi surface curvature, which does not necessarily correspond to the number of carriers (band filling). Thus, we believe that the chemically determined carrier density is a more reasonable parameter to analyze the physical properties of this system. For $x \neq 1$ samples, we cannot calculate the doped carrier density precisely because the oxygen content has not been determined. However, the resistivity data of $TlSr_2(Lu_{1-x}Ca_x)Cu_2O_y$ suggest that hole carriers increase with the Ca content $x$ or the oxygen content $y$.[11] Thus, we confirmed, qualitatively in the underdoped regime and quantitatively in the overdoped regime, the bell-shaped behavior of $T_c$ vs doping, which is commonly observed in high-$T_c$ cuprates.

## IV. NORMAL-STATE MAGNETIC SUSCEPTIBILITY

The temperature dependence of the normal-state magnetic susceptibility $\chi$ was measured at 10 kOe using the same samples for which we determined the $T_c$ values. Figures 5(a) and 5(b) demonstrate the data corrected for the core diamagnetic susceptibility $\chi_{core}$ of the oxygenated and argon-reduced samples, respectively. The $\chi_{core}$ value is about $-9\times10^{-5}$ emu/mol Cu, which is calculated using tabulated values[14] and depends slightly on $x$. The reversibility of the change in $\chi$ versus oxygen content was confirmed for all samples. In Fig. 5(b), the data for the $x=0$ and $x=1.0$ oxygenated samples are also given for comparison.

In Fig. 5(a), it is noted that Curie-like upturns are observed at low temperature for both insulating ($x=0$) and overdoped metallic ($x=1.0$) samples. If these Curie-like components are assumed to arise from $Cu^{2+}$ spins, the ratios of $Cu^{2+}$ to all Cu atoms are estimated to be at most 0.5% and 0.2%, respectively. However, it is difficult to determine whether such small Curie terms are intrinsic or due to undetectable small impurities.

When the preparation condition differs from the optimal one, as described in Sec. II, the obtained samples often contain some impurities: Sr(Ca)-Cu oxides[15,16] and Tl-Sr(Ca) oxides. Since the latter oxides do not contain Cu, their magnetic susceptibilities are mainly due to the core diamagnetism, and are small enough to be neglected. The former oxides include $Sr_2CuO_3$,[17] $Sr(Ca)_{14}Cu_{24}O_{41}$,[18,19] and $SrCuO_2$,[17] and the magnetic

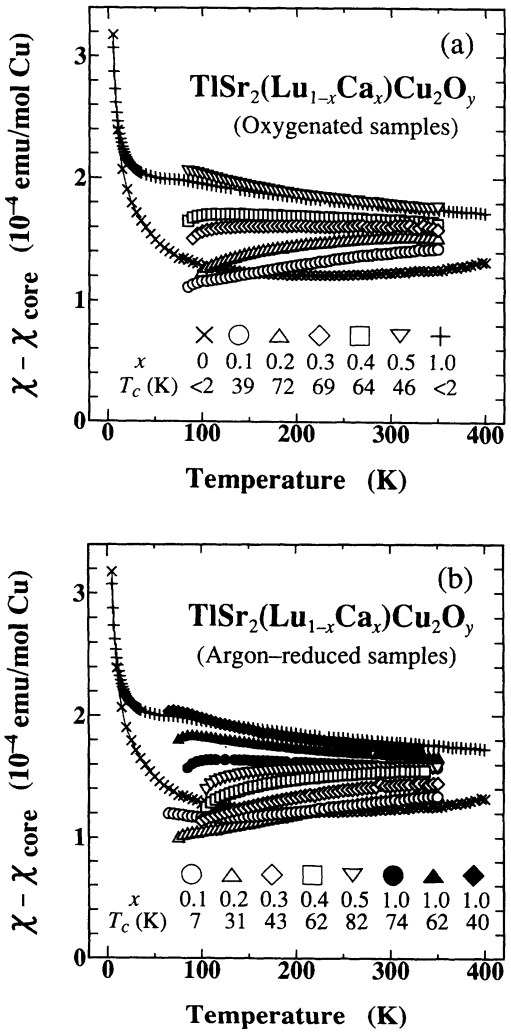


FIG. 5. Temperature dependence of the magnetic susceptibility after correction for $\chi_{core}$ of $TlSr_2(Lu_{1-x}Ca_x)Cu_2O_y$ with $0 \leq x \leq 0.5$ and $x=1.0$: (a) oxygenated at 350 °C and (b) argon reduced at 550 °C. In (b) the $x=1.0$ sample was argon reduced at 350 °C (♦), 450 °C ( ▲ ), and 550 °C (●). Data for the $x=0$ ( × ) and $x=1.0$ ( + ) oxygenated samples are also shown.

susceptibilities after correcting for $\chi_{core}$ of these oxygenated compounds are shown in Fig. 6. Though the magnetic susceptibility of $SrCuO_2$ is small enough to be neglected, the others show remarkable Curie-like behavior. The $\chi$ data for $Sr_2CuO_3$ are well fitted to the Curie-Weiss law with a small Weiss temperature of $-2.1$ K over the entire temperature range. The ratio of $Cu^{2+}/Cu$ is estimated as 12%. $Sr_{14}Cu_{24}O_{41}$ shows more complicated temperature dependence of $\chi$, which below 25 K can be fitted to the Curie law with a $Cu^{2+}/Cu$ ratio of 5% but which above 25 K shows a larger negative slope than predicted by the Curie law.

Because no impurities were detected by either the x-ray diffraction or the SEM-EPMA technique, the amount of impurities, if any, in our samples is less than a few percent. Therefore, $Sr_2CuO_3$ and $Sr(Ca)_{14}Cu_{24}O_{41}$ may be the impurities that produce the small Curie-like components with the $Cu^{2+}/Cu$ ratio of 0.2–0.5 %. In fact, for some $x=1.0$ samples we found a quantitative correlation between the magnitude of the Curie term and the volume fraction of impurities like $Sr_2CuO_3$ and $Sr(Ca)_{14}Cu_{24}O_{41}$. These samples were prepared under nonoptimal conditions and thus contained detectable amounts of impurities. This suggests that the small Curie-like components for both $x=0$ and $x=1.0$ oxygenated samples are not intrinsic but are instead due to undetectably small amounts of impurities. For the $x=0.1$ aron-reduced sample ($T_c=7$ K), however, a Curie-like upturn is also observed below 150 K, whereas for the $x=0.1$ oxygenated sample ($T_c=39$ K), it is not. This might indicate that the Curie term in the insulating phase is not due to impurities but is intrinsic.

In any case, it should be noted that a Curie term as small as that of the $x=1.0$ oxygenated sample has little effect on the $\chi(T)$ data above 100 K. Above 40 K the $\chi(T)$ data for the $x=1.0$ oxygenated sample shows a larger negative slope than predicted by the Curie law,

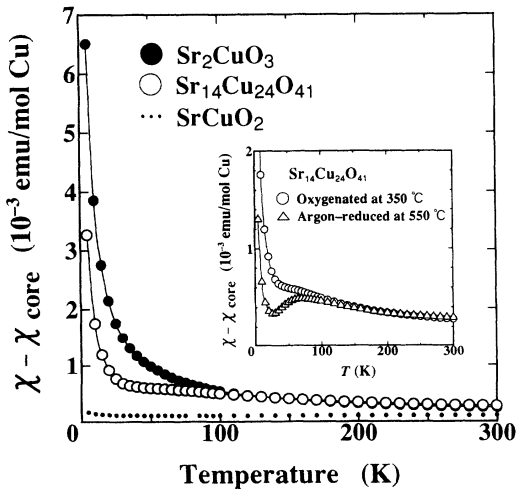


FIG. 6. Temperature dependence of the magnetic susceptibility after correction for $\chi_{core}$ of $Sr_2CuO_3$, $Sr_{14}Cu_{24}O_{41}$, and $SrCuO_2$ oxygenated at 350 °C. The inset shows the data for $Sr_{14}Cu_{24}O_{41}$ argon reduced at 550 °C, together with those for the oxygenated one.

which resembles that for the oxygenated $Sr_{14}Cu_{24}O_{41}$ as shown in Fig. 6. However, this is not due to the existence of $Sr_{14}Cu_{24}O_{41}$ because for $Sr_{14}Cu_{24}O_{41}$ the negative slope above 100 K is almost unchanged by argon reduction. This is shown in the inset of Fig. 6, which is in contrast to the results for the $x=1.0$ argon-reduced samples shown in Fig. 5(b). Thus the negative slope of $\chi(T)$ above 100 K seems to be an essential characteristic of the $x=1.0$ oxygenated sample. Such negative temperature dependence of $\chi$ might be universal in the highly overdoped regime because the Knight shift of the overdoped $La_{2-x}Sr_xCuO_4$ is found to increase with decreasing temperature.[20,21]

Therefore, if the Curie-like component for each sample is as small as that for the $x=1.0$ oxygenated sample, the $\chi(T)$ data above 100 K in Figs. 5(a) and 5(b) are considered to exhibit the essential behaviors of the magnetic susceptibility in this system. We next analyze the $\chi(T)$ data above 100 K.

In a normal metal, $\chi$ is generally expressed as

$$\chi=\chi_{spin}+\chi_L+\chi_{orb}+\chi_{core}\ , \tag{1}$$

where $\chi_{spin}$, $\chi_L$, $\chi_{orb}$, and $\chi_{core}$ are the spin susceptibility, Landau diamagnetic susceptibility, Van Vleck orbital susceptibility, and core diamagnetic susceptibility, respectively. $\chi_{orb}$ can be estimated by the $^{63}$Cu Knight-shift data.[22] In general, the Knight shift $K$ is the sum of the spin and orbital parts:

$$K=K_{spin}+K_{orb}\ , \tag{2}$$

where $K$ due to $\chi_{core}$ is neglected.[23] The relation between $K_{orb}$ and $\chi_{orb}$ obeys the following equation:

$$K_{orb}=A_{orb}\chi_{orb}/N_A\mu_B\ , \tag{3}$$

where $A_{orb}$, $N_A$, and $\mu_B$ are the hyperfine field, Avogadro's number, and the Bohr magneton, respectively. If we assume that $^{63}K_{spin}=0$ at $T=0$,[24] then $^{63}K_{orb}$, which is independent of temperature, is given by extrapolating the $^{63}K$ data to 0 K. From Ref. 22 we can estimate for $TlSr_2CaCu_2O_y$ that $^{63}K_{orb}^{(ab)}\approx 0.25\%$ and that $^{63}K_{orb}^{(c)}\approx 1.2\%$, where $(ab)$ and $(c)$ represent the field directions in the $ab$ plane and parallel to the $c$ axis, respectively. These values are close to those for other high-$T_c$ cuprates, such as $YBa_2Cu_3O_{6.63}$,[25] $YBa_2Cu_3O_7$,[26] $Bi_2Sr_2CaCu_2O_8$,[27] and $Tl_2Ba_2CuO_{6+\delta}$,[28] suggesting that the $^{63}K_{orb}$ values of high-$T_c$ cuprates are almost the same from the underdoped to the overdoped regimes. We assume here that the $^{63}K_{orb}$ values for $TlSr_2(Lu_{1-x}Ca_x)Cu_2O_y$ are identical at every substitution level $x$. If we then use the theoretical estimate of $A_{orb}$,

$$A_{orb}=2\mu_B\langle r^{-3}\rangle\ , \tag{4}$$

where $\langle r^{-3}\rangle$ is taken to be 6.3 a.u.,[29] we obtain $\chi_{orb}^{(ab)}\approx 1.8\times10^{-5}$ and $\chi_{orb}^{(c)}\approx 8.5\times10^{-5}$ emu/mol Cu for the $TlSr_2(Lu_{1-x}Ca_x)Cu_2O_y$ system. Thus the powder average value of $\chi_{orb}$ is

$$\langle\chi_{orb}\rangle=(2\chi_{orb}^{(ab)}+\chi_{orb}^{(c)})/3\approx 4.0\times10^{-5}\text{emu/mol Cu}\ . \tag{5}$$

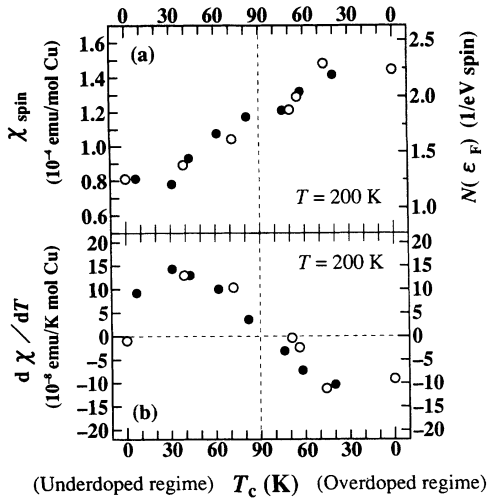


FIG. 7. (a) $\chi_{spin}$ values at 200 K and (b) $d\chi/dT$ values at 200 K of $TlSr_2(Lu_{1-x}Ca_x)Cu_2O_y$ plotted versus $T_c$ values. Open and closed circles represent samples oxygenated at 350° and argon reduced at 550°C, respectively. The $T_c$ values are classified into the underdoped (left) and the overdoped (right) regimes (see text).

For a free-electron gas with effective mass $m^*$,

$$\chi_L = -(m_e/m^*)^2\chi_{spin}/3 , \quad (6)$$

where $m_e$ is the free-electron mass. Since the effective mass is observed to be enhanced more than twofold in the cuprate superconductors,[30] $\chi_L$ will be neglected in this analysis.

Using the above analysis we can estimate $\chi_{spin}$ of $TlSr_2(Lu_{1-x}Ca_x)Cu_2O_y$. In Fig. 7(a), the estimated $\chi_{spin}$ values at 200 K for the samples shown in Figs. 5(a) and 5(b) are plotted versus $T_c$ values. The data shown in this figure are classified into the underdoped and the overdoped regimes, and respectively plotted in the left half (0–90 K) and the right half (90–0 K) of the figure. From the bell-shaped dependence of $T_c$ on the carrier doping, the horizontal axis is considered to roughly scale the carrier density. As the hole carrier is doped, the $\chi_{spin}$ values increase monotonically from the underdoped to the overdoped regime. This seems to show that there is no discontinuity in the magnetism from the underdoped to the overdoped regime. The $\chi_{spin}$ value at the optimum doping is estimated to be $1.2\times10^{-4}$ emu/mol Cu. The corresponding density of states at the Fermi surface $N(\varepsilon_F)$, obtained using the relation $\chi=2\mu_B^2N(\varepsilon_F)/N_A$, is about 1.8 states per eV Cu spin. This value is about twice as large as that predicted by the band-structure calculations for the other high-$T_c$ cuprates,[31] and is close to the $\chi_{spin}$ values estimated for $YBa_2Cu_3O_7$,[32,33] $Bi_2Sr_2CaCu_2O_{8+\delta}$,[34] and $Tl_2Ba_2CuO_{6+\delta}$ ($T_c=79$ K),[8] if $\chi_{orb}$ for each high-$T_c$ cuprate is estimated using each $^{63}K$ as described above.

Figures 5(a) and 5(b) seem to indicate that the slope of $\chi(T)$ above 100 K gradually changes from positive to negative with doping, and that $\chi(T)$ becomes nearly temperature independent for optimally doped samples. This trend is clarified by plotting the slope $d\chi/dT$ at 200 K for each sample versus $T_c$ [see Fig. 7(b)]. The slope changes successively and systematically from the underdoped to the overdoped regime with doping, and is almost entirely temperature independent at the optimum carrier density. Such behavior is also observed in the one-side regime for other high-$T_c$ cuprate systems, such as $YBa_2Cu_3O_{7-\delta}$,[35] $Bi_2Sr_2(Y_{1-x}Ca_x)Cu_2O_{8+\delta}$,[36] and $Tl_2Ba_2CuO_{6+\delta}$.[8] These characteristics of $\chi(T)$ thus seem to be typical of high-$T_c$ cuprates and to be closely related to the high-$T_c$ superconductivity mechanism.

## V. CONCLUSION

Single-phase $TlSr_2(Lu_{1-x}Ca_x)Cu_2O_y$ samples ($0\le x\le1.0$) were prepared by solid-state reaction, starting with Tl-rich compositions and measuring the sample weight. In this system, hole carriers are doped by the Ca substitution $x$. When $x$ increases from 0 to 1.0, the oxygenated sample changes from an insulator ($x=0$) to a nonsuperconducting metal ($x=1.0$), by way of a superconductor showing a maximum $T_c$ value at $x=0.2$. The $T_c$ values are significantly changed by argon reduction, which decreases the hole carrier density by reducing the oxygen content $y$. The samples for which $x\le0.2$ and $x\ge0.6$ are found to belong to the underdoped and the overdoped regimes, respectively. For $0.3\le x\le0.5$, the $T_c$ value shows a crossover behavior from the underdoped to the overdoped regime and has a maximum value at an intermediate oxygen content.

The normal-state magnetic susceptibility $\chi$ of these samples was evaluated as a function of Ca concentration $x$ and oxygen content $y$. For nonsuperconducting samples ($x=0$ and $x=1.0$), small Curie-like upturns are observed at low temperature. Although it is not yet clear whether they are intrinsic or not, they have little effect on the $\chi$ data above 100 K. The correlation between the $\chi(T)$ data above 100 K and the carrier density ($T_c$ value) is found to have two significant characteristics. One is that the slope of the $\chi(T)$ curve gradually changes from positive to negative on going from the underdoped to the overdoped regime and is almost entirely independent of temperature at the optimum carrier density ( maximum value of $T_c$). The other is that the magnitude of the estimated spin susceptibility $\chi_{spin}$ at 200 K increases with the carrier density and is about $1.2\times10^{-4}$ emu/mol Cu for the optimum carrier density. These two characteristics are typical of most high-$T_c$ cuprates and seem to be closely related to the high-$T_c$ superconductivity mechanism.

## ACKNOWLEDGMENTS

We thank Hitoshi Igarashi and Masashi Mizuta for their support during this work.

[1]J. B. Torrance, Y. Tokura, A. I. Nazzal, A. Bezinge, T. C. Huang, and S. S. P. Parkin, Phys. Rev. Lett. **61**, 1127 (1988).
[2]J. D. Jorgensen, P. Lightfoot, S. Pei, B. Drabrowski, D. R. Richards, and D. G. Hinks, in *Advances in Superconductivity III,* edited by K. Kajimura and H. Hayakawa (Springer-Verlag, Tokyo, 1991), p. 337.
[3]H. Takagi, R. J. Cava, M. Marezio, B. Batlogg, J. J. Krajewski, W. F. Peck, Jr., P. Bordet, and D. E. Cox, Phys. Rev. Lett. **68**, 3777 (1992).
[4]Y. Shimakawa, Y. Kubo, T. Manako, and H. Igarashi, Phys. Rev. B **40**, 11 400 (1989).
[5]Y. Shimakawa, Y. Kubo, T. Manako, H. Igarashi, F. Izumi, and H. Asano, Phys. Rev. B **42**, 10 165 (1990).
[6]F. Izumi, T. Kondo, Y. Shimakawa, T. Manako, Y. Kubo, H. Igarashi, and H. Asano, Physica C **185-189**, 615 (1991).
[7]Y. Kubo, T. Kondo, Y. Shimakawa, T. Manako, and H. Igarashi, Phys. Rev. B **45**, 5553 (1992).
[8]Y. Kubo, Y. Shimakawa, T. Manako, and H. Igarashi, Phys. Rev. B **43**, 7875 (1991).
[9]T. Manako, Y. Kubo, and Y. Shimakawa, Phys. Rev. B **46**, 11 019 (1992).
[10]Y. Kubo and T. Manako, Physica C **197**, 378 (1992).
[11]T. Kondo, Y. Kubo, Y. Shimakawa, T. Manako, and H. Igarashi, Physica C **185-189**, 669 (1991).
[12]T Doi, K. Usami, and T. Kamo, Jpn. J. Appl. Phys. **29**, L57 (1990).
[13]F. Izumi, J. Crystallogr. Soc. Jpn. **27**, 23 (1985).
[14]R. R. Gupta, in *Diamagnetic Susceptibility,* edited by K.-H. Hellwege and A. M. Hellwege, Landolt-Börnstein, New Series, Group II Vol. 16 (Springer-Verlag, Heidelberg, 1986), p. 402.
[15]R. S. Roth, C. J. Rawn, J. D. Whitler, C. K. Chiang, and W. K. Wong-Ng, J. Am. Ceram. Soc. **72**, 395 (1989).
[16]Y. Ikeda, H. Ito, S. Shimomura, Z. Hiroi, M. Takano, Y. Bando, J. Takada, K. Oda, H. Kitaguchi, Y. Takeda, and T. Takada, Physica C **190**, 18 (1991).
[17]H. Ohta, N. Yamauchi, M. Motokawa, M. Azuma, and M. Takano, J. Phys. Soc. Jpn. **61**, 3370 (1992).
[18]E. M. McCarron, III, M. A. Subramanian, J. C. Calabrese, and R. L. Harlow, Mater. Res. Bull. **23**, 1355 (1988).
[19]T. Siegrist, L. F. Schneemeyer, S. A. Sunshine, and J. V. Waszczak, Mater. Res. Bull. **23**, 1429 (1988).
[20]G.-Q. Zheng, T. Kuse, Y. Kitaoka, K. Ishida, S. Ohsugi, K. Asayama, and Y. Yamada, Physica C **208**, 339 (1993).
[21]Y.-Q. Song, M. A. Kennard, K. R. Poeppelmeier, and W. P. Halperin, Phys. Rev. Lett. **70**, 3131 (1993).
[22]G.-Q. Zheng, K. Magishi, Y. Kitaoka, K. Asayama, T. Kondo, Y. Shimakawa, T. Manako, and Y. Kubo, Physica B **186-188**, 1012 (1993).
[23]Y. Yoshinari, H. Yasuoka, Y. Ueda, Kei-ichi Koga, and K. Kosuge, J. Phys. Soc. Jpn. **59**, 3698 (1990).
[24]M. Takigawa, P. C. Hammel, R. H. Heffner, Z. Fisk, J. L. Smith, and R. B. Schwarz, Phys. Rev. B **39**, 300 (1989).
[25]M. Takigawa, A. P. Reyes, P. C. Hammel, J. D. Thompson, R. H. Heffner, Z. Fisk, and K. C. Ott, Phys. Rev. B **43**, 247 (1991).
[26]M. Takigawa, P. C. Hammel, R. H. Heffner, and Z. Fisk, Phys. Rev. B **39**, 7371 (1989).
[27]R. E. Walstedt, R. F. Bell, and D. B. Mitzi, Phys. Rev. B **44**, 7760 (1991).
[28]Y. Kitaoka, K. Fujiwara, K. Ishida, K. Asayama, Y. Shimakawa, T. Manako, and Y. Kubo, Physica C **179**, 107 (1991).
[29]A. Abragam and B. Bleaney, *Electron Paramagnetic Resonance of Transition Ions* (Clarendon, Oxford, 1970), Sec. 7.16.
[30]J. W. Loram, K. A. Mirza, J. R. Cooper, and W. Y. Liang, Phys. Rev. Lett. **71**, 1740 (1993).
[31]W. E. Pickett, Rev. Mod. Phys. **61**, 433 (1989).
[32]F. Mila and T. M. Rice, Physica C **157**, 561 (1989).
[33]R. E. Walstedt and W. W. Warren, Jr., Science **248**, 1082 (1990).
[34]W. C. Lee, J. H. Cho, and D. C. Johnston, Phys. Rev. B **43**, 457 (1991).
[35]Y. Nakazawa and M. Ishikawa, Physica C **158**, 381 (1989).
[36]T. Tamegai, K. Koga, K. Suzuki, M. Ichihara, F. Sakai, and Y. Iye, Jpn. J. Appl. Phys. **28**, L112 (1989).